BUTTERWORTH HEINEMANN

0141-0296(95)00103-4

Engineering Structures, Vol. 17, No. 7, pp. 485–493, 1995

0141-0296/95 $10.00 + 0.00

Inelastic response of the Cypress Viaduct to the Loma Prieta earthquake

Sashi K. Kunnath

Department of Civil and Environmental Engineering, University of Central Florida, Orlando, FL 32816-2450, USA

John L. Gross

Building and Fire Research Laboratory, National Institute of Standards and Technology, Gaithersburg, MD, 20899, USA

(Received May 1994; revised version accepted August 1994)

The inelastic damage evaluation of a typical double-deck bent of the Cypress Viaduct which collapsed during the 1989 Loma Prieta earthquake is presented. A model of the bent consisting of spread plasticity-based beam-column elements to represent the piers and deck, and shear panel elements to represent the pedestal region was developed. To accurately determine beam and column moment–curvature relationships, separate computer analyses using an element fibre model were conducted. In addition, a smeared-crack approach finite element analysis was employed to determine the lateral load–deformation relationship of the pedestal regions. The model of the Cypress Viaduct was subjected to the Oakland Outer Harbor Wharf ground acceleration record in the plane of the bent. The analytical model was calibrated using static lateral load tests, ambient and forced vibration tests, and observed performance. The results of time-history analyses, which include a prediction of member damage, indicate that collapse was initiated by a shear failure of the pedestal regions.

Keywords: bridges, damage evaluation, dynamic response, elevated highway structures, failure analysis, modelling, reinforced concrete, seismic analysis

The Loma Prieta earthquake provided researchers with valuable data on the performance of structures against which analytical models could be validated. The Cypress Viaduct (or Interstate I880) which collapsed during the earthquake, provides an excellent opportunity to evaluate and, if necessary, improve upon current analytical procedures that attempt to predict damage and limit states of reinforced concrete structures subjected to strong earthquakes. This study attempts to investigate if it would have been possible to predict the imminent failure of the structure using computer-based analysis methods in which system characteristics are prescribed as accurately as possible.

The inelastic damage analysis program IDARC[1,2] was used as the base analytical platform for the study. Among the basic features that made IDARC suitable for this evaluation were: (i) a distributed flexibility model to represent implicitly the spread of plasticity; (ii) a versatile hysteretic force–deformation model which could represent stiffness degradation, strength deterioration, and pinching effects; and (iii) a shear panel element with capability to model inelastic flexure and shear independently. Some modifications were necessary to enable the complete nonlinear analysis of the double-deck bent under combined static and seismic loading. The revised program was used in extensive analytical evaluations of a typical bent that failed during the earthquake. Details of the formulations and analyses are summarized in this paper.

1. Description of the Cypress Viaduct

The Cypress Viaduct, a two-mile elevated section of the Nimitz Freeway, was part of a major interstate highway (I880) linking Oakland with the San Francisco–Oakland Bay Bridge. It was located approximately 100 km from the epicentre of the earthquake. The double-deck viaduct carried four lanes of northbound traffic on the lower level and

four lanes of southbound traffic on the upper level. The upper and lower level box girder roadway decks were supported by 83 reinforced concrete bents. There were 11 different bent configurations, and of the 48 bents that collapsed, 29 (or 60%) were type B1 bents. In this study, only the type B1 bent is considered.

Type B1 bents consisted essentially of two portal frames, one on top of the other. Typical dimensions for the type B1 bent are shown in *Figure 1*. Above the lower level transverse beam were short column sections, 0.69 m (27 in) high, referred to here as pedestals. The upper portal frame was supported on top of the pedestals and connected by means of a shear key, which provided essentially no moment resistance. The columns of the upper portal frame were tapered, ranging from 0.91 m (36 in) deep at the bottom to 1.22 m (48 in) at the top and were 1.22 m (48 in) wide. The upper level transverse beam had the same dimensions as the lower beam. The reinforcement layout for the type B1 bent is shown in *Figure 2*. The roadway deck was a reinforced concrete cellular box girder. For the purposes of computing dead weight, the box girder was assumed to be surfaced with 127 mm (5 in) of asphalt.

The bents were supported on pile caps ranging from 0.91 to 1.52 m (36 to 54 in) thick. The pile caps were in turn supported on 305 mm (1 ft) diameter concrete-filled pipe piles. The number of piles at each column varied, ranging from 18 to 35 piles. The connection between the first-level columns and the pile caps was a structural hinge. Complete details of the bent configuration and the layout of the viaduct can be found in separate reports[3,4].

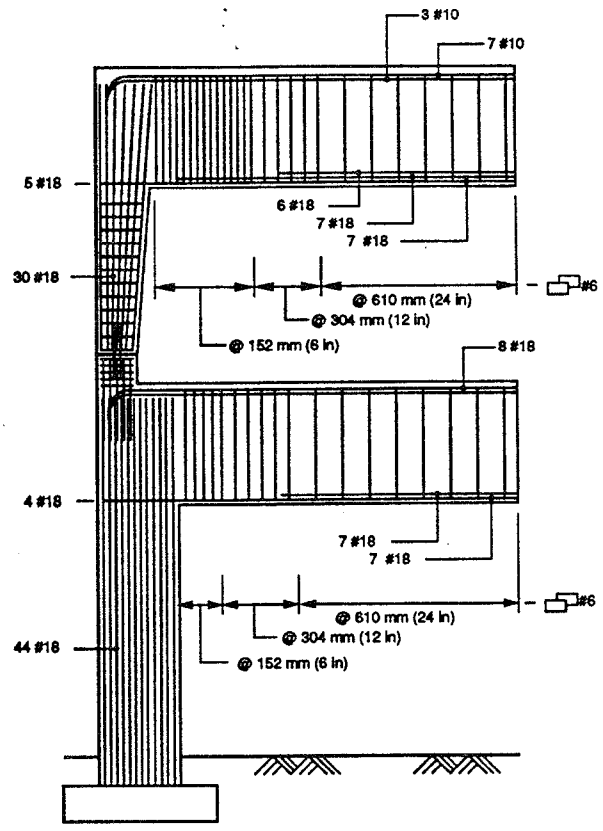

Figure 2 Reinforcement layout for typical B1 bent

2. Modelling of type B1 bent

The Cypress Viaduct was modelled as an assemblage of prismatic and tapered members as shown in *Figure 3*. The upper level tapered columns were modelled as vertical elements and the lower level columns were assumed to be collinear with the upper level columns. Rigid links were used to model the joint regions with the exception of the pedestal region. Hinges were used to model the base fixity condition and the joints between the pedestals and upper level columns while all other joints were assumed to be rigid. Six prismatic members were used to describe the beams. This was done to permit each beam to respond to vertical accelerations in flexure since lumped masses were assigned to each node. The beam elements have transverse and rotational degrees of freedom only (no axial deformations). The columns were modelled as single elements, prismatic for the lower level and tapered for the upper level. The columns have axial, transverse and rotational degrees of freedom. The pedestals were modelled with shear wall panel elements in which both inelastic shear and flexural deformations are included.

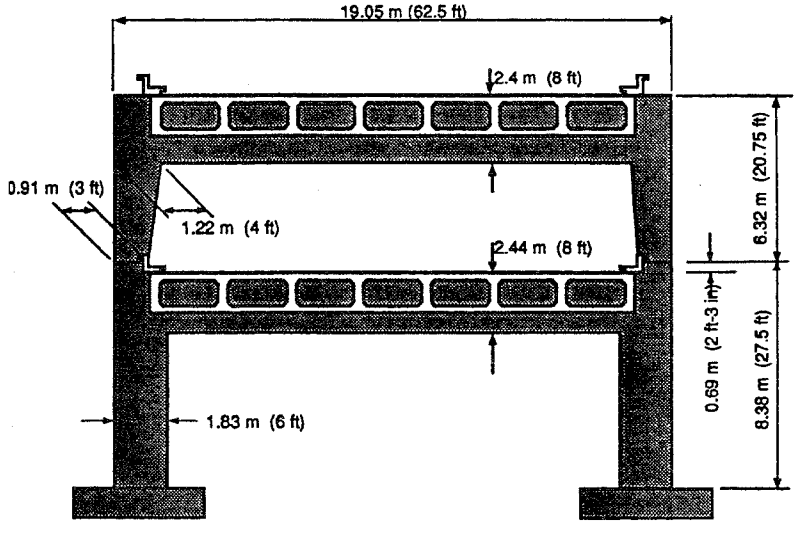

Figure 1 Typical dimensions of type B1 bent

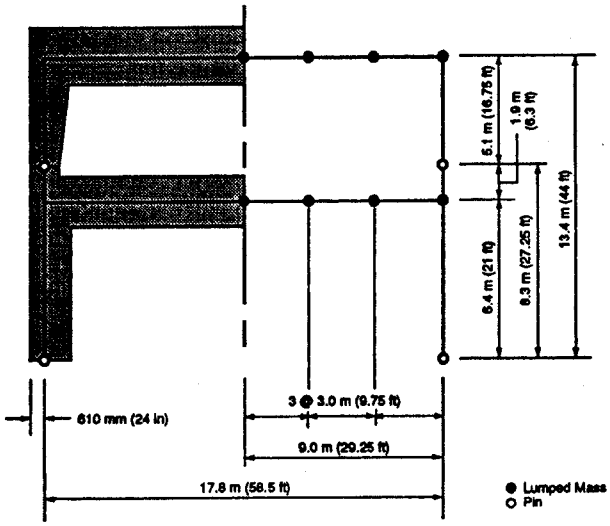

Figure 3 IDARC model of type B1 bent

2.1. *Component modelling*

A typical beam-column element is shown in *Figure 4* identifying the rigid panel zones and the end rotations. Since significant cracking and yielding of the members are expected, with inelastic deformations propagating into the member, it is essential to consider a member model in which the effects of spread plasticity are incorporated. Such models are typically based on flexibility formulations, wherein the flexibility distribution along the member length is assumed to have a predetermined form. In the original IDARC program, the flexural rigidity, $1/EI$, is assumed to vary linearly for prismatic members with constant cross-sections. If the flexural rigidity, EI, at the ends of the member is monitored throughout the analysis, the incremental moment–rotation relationship can be established from direct integration of the (M/EI) diagram. The flexibility matrix is expressed in the following incremental form

$$\begin{Bmatrix} \Delta\theta'_A \\ \Delta\theta'_B \end{Bmatrix} = [f_S] \begin{Bmatrix} \Delta M'_A \\ \Delta M'_B \end{Bmatrix} \tag{1}$$

where $\Delta\theta'_A$, $\Delta\theta'_B$ are the incremental rotations corresponding to the moment increments $\Delta M'_A$, $\Delta M'_B$. The advantage of a linear distribution of flexibility is that it is possible to derive the flexibility coefficients in closed form and thus simplify the numerical effort required during the analysis[1].

A new distributed flexibility formulation was derived for tapered prismatic members. Again, to simplify the numerical computations, the moment of inertia is assumed to vary linearly along the member length, resulting in the flexural rigidity varying nonlinearly as shown in *Figure 5*. However, a numerical integration along the member is required to evaluate the flexibility coefficients. The flexibility coefficients are obtained from the following integrals

$$f_{11} = \int_0^L \frac{1}{EI_x}\left(1 - 2\frac{x}{L} + \frac{x^2}{L^2}\right) dx \tag{2}$$

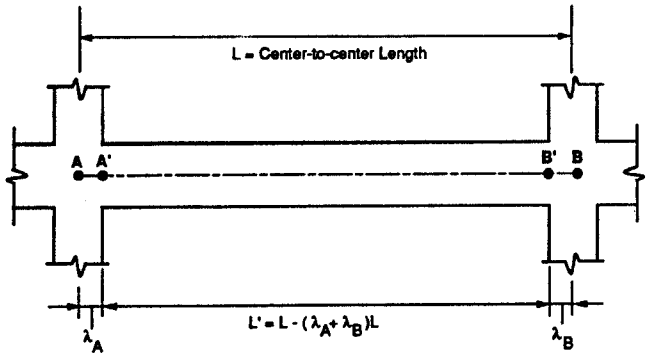

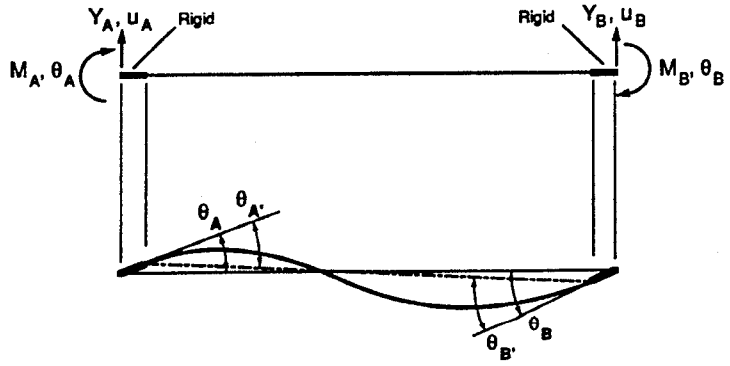

Figure 4 Typical component model showing rigid end zones

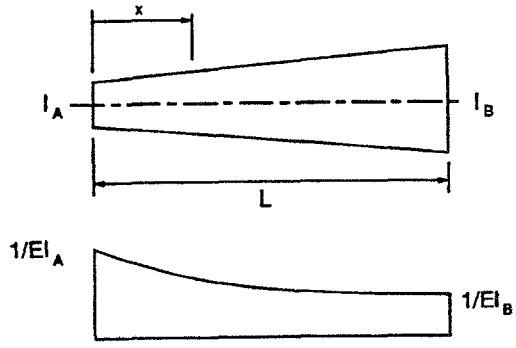

Figure 5 Assumed flexibility distribution for tapered members

$$f_{12} = -f_{21} = \int_0^L \frac{1}{EI_x}\left(-\frac{x}{L} + \frac{x^2}{L^2}\right) dx \tag{3}$$

$$f_{22} = \int_0^L \frac{1}{EI_x}\left(\frac{x^2}{L^2}\right) dx \tag{4}$$

where

$$\frac{1}{EI_x} = \frac{1}{EI_A} + \frac{x}{L}\left(\frac{1}{EI_B} - \frac{1}{EI_A}\right) \tag{5}$$

The above formulation was used for the two tapered columns in the upper level of the bent only. The linear flexibility model of IDARC for regular prismatic members with constant cross-sections was used for all other elements.

2.2. *Hysteretic modelling*

Nonlinear behaviour is prescribed through hysteretic force–deformation modelling. IDARC includes a versatile hysteretic model in which a nonsymmetric trilinear envelope, in conjunction with three user-specified parameters, is used to produce the effects of stiffness degradation, strength deterioration and pinching. Stiffness degradation is controlled by the parameter, α, and is achieved by reducing the unloading stiffness as a function of ductility. Strength deterioration, controlled by the parameter, β, is introduced as a function of dissipated hysteretic energy. Finally, pinching or slip behaviour (caused by crack-closing) is incorporated by lowering the target point of the force–deformation curve upon crossing the force-axis through the control parameter, γ. The hysteretic loop behaviour illustrating each of the above effects is shown in *Figure 6*. Details of the implementation of the hysteretic model can be found in Park *et al*[5]. The three parameters can be combined in a variety of ways to produce a range of hysteretic behaviours. Default values of the three parameters were used in the present analysis, since it was found that the collapse condition was caused by sudden large inelastic deformations (as opposed to several cycles of dissipated hysteretic energy) and even significant variations in the hysteretic parameters did not change the failure mode. A representative set of hysteresis loops produced by the default set of parameters is also shown in *Figure 6*.

2.3. *Solution strategies*

The incremental solution of the assembled system of equations involves the following dynamic equation of equilibrium

$$[K]\{u\} = \{R\} \tag{6}$$

in which $[K]$ is the assembled stiffness matrix, $\{u\}$ is the unknown displacement vector, and $\{R\}$ is the equivalent dynamic force applied at each step of the analysis. The solution of equation (6) is accomplished by a direct step-by-step integration procedure using Newmark's unconditionally stable constant average acceleration method. The step-by-step procedure assumes that the properties of the structure do not change during the time step of analysis. However, since the stiffness of some element is likely to change state during some calculation step, the new configuration may not satisfy equilibrium. A compensation procedure is adopted to minimize this error by applying a single-step unbalanced force correction.

The use of a distributed flexibility model and the multilinear hysteretic force–deformation model present formidable challenges in element state determination. The flexibility matrix for a member needs to be updated for one or both of the following reasons: (i) a transition in stiffness as prescribed by the hysteresis model; and (ii) a shift in the contraflexure point. All such changes lead to unbalanced forces between two solution steps. Item (i) can be dealt with using an event-to-event strategy which can be extremely time-intensive. The difficulties associated with a varying contraflexure point are not associated with any predefined event change. Hence, an iterative approach to ensure stability of the final solution is necessary. To expedite the solution process, the initial contraflexure points (not necessarily at the centre of the member) computed for each element at the first load step of the analysis are used throughout the analysis.

All unbalanced forces are added at the start of the next step and removed subsequently to prevent the accumulation of erroneous external forces. Such an unbalanced force correction is typically applied only to the moments, since they represented the primary yielding mechanism. However, in the present analysis of the Cypress Viaduct, a significant source of inelastic behaviour comes from the pedestal regions, modelled in this study as shear wall elements. The correction of unbalanced moments caused by shear failure is not straightforward. The following procedure was devised to include this correction:

Assume that, at time t_i the moments at ends A and B are M_A and M_B, respectively. At time step t_{i+1}, let the incremental moments at the ends be ΔM_A and ΔM_B. This gives rise to an incremental shear, $\Delta V = V_{i+1} - V_i$, given by $(\Delta M_A - \Delta M_B)/L$ using the sign convention shown. If this incremental shear causes a change of state in the shear spring, the hysteretic model returns an unbalanced force, ΔV_e, as illustrated in *Figure 7*. Corrective moments are then applied resulting in corrected incremental moments, ΔM_A^* and ΔM_B^*, as follows

$$\Delta M_A^* = \Delta M_A - C_f \Delta V_e \tag{7}$$

$$\Delta M_B^* = \Delta M_B - (1 - C_f)\,\Delta V_e \tag{8}$$

where

$$C_f = \frac{M_A}{(M_A - M_B)} L \tag{9}$$

The unbalanced forces are computed when moments, shears and stiffnesses are being updated in the hysteretic

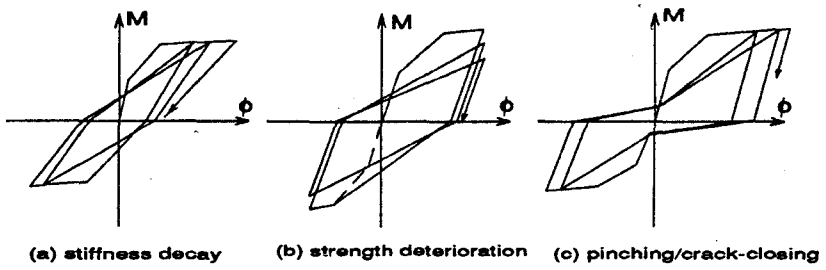

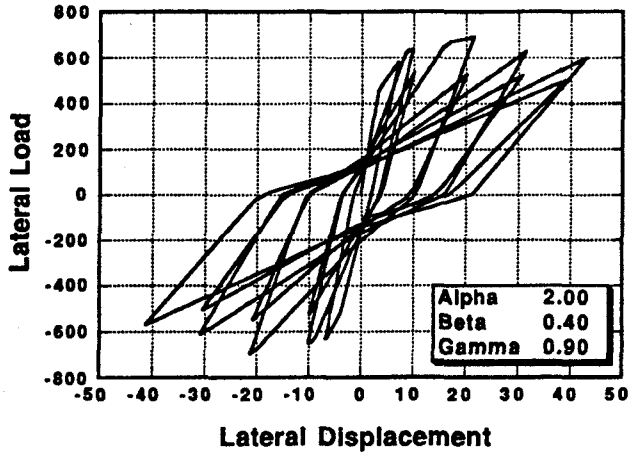

Figure 6 Modelling of hysteresis behaviour: stiffness degradation, strength loss, and pinching (above); typical loops for assumed hysteretic parameters (below)

model. Such a procedure is preferable over a fully iterative nonlinear analysis since the computing time for the latter would become prohibitive, especially for large building systems.

2.4. *Damage modelling*

A qualitative measure of the inelastic response was expressed in terms of a damage index. The damage model in the original release version of IDARC is that developed by Park *et al.*[6] wherein the structural component damage, D_c, is expressed as a linear combination of the ductility (deformation) damage and that contributed by hysteretic energy dissipation due to repeated cyclic loading. Direct application of the model to structural systems requires determination of an overall member deformation. Since inelastic behaviour is confined within plastic zones near the ends of a member, the relationship between overall member deformation, local plastic rotations and the damage index is difficult to correlate. Moreover, the presence of internal member hinges (as is the case in the Cypress structure) renders the model unusable. Therefore, a modified version of the component damage model was used, based on moment and curvature, as follows

$$D_c = \frac{\phi_m - \phi_r}{\phi_u - \phi_r} + \frac{\beta}{M_y \phi_u} A_T \qquad (10)$$

where

ϕ_m maximum curvature attained during load history
ϕ_u ultimate curvature capacity of section
ϕ_r recoverable curvature at unloading
β strength degrading parameter
M_y yield moment of section
A_T total area contained in $M - \phi$ loops

The quantity A_T does not correspond to the original energy term in Park's model. However, it does represent an implicit measure of energy, and when normalized as indicated above, was found to correlate fairly well with the original strength-degrading parameter, β.

2.5. *Evaluation of member properties*

The trilinear moment–curvature or force–deformation relationship at each member end is required as input to the inelastic seismic analysis. Determination of these relationships for beams and columns was obtained through accurate fibre model analysis of each cross-section. A parabolic concrete stress–strain relationship and a linear elastic-perfectly-plastic relationship for the longitudinal reinforcement was used. The procedure involves the increment of compressive strains while the corresponding stress distribution is computed such that equilibrium is satisfied. The stresses are integrated to produce the moment on the section, and the compressive strain and location of neutral axis give the corresponding curvature. The resulting moment–curvature relationship and the assumed trilinear representation for a typical element are shown in *Figure 8*. Computed member properties for both beam and column sections using the fibre model analysis are summarized in *Tables 1* and *2*, respectively.

The pedestals were modelled as shear wall elements since shear deformations were expected to be significant. The shear wall element in IDARC requires the shear load–

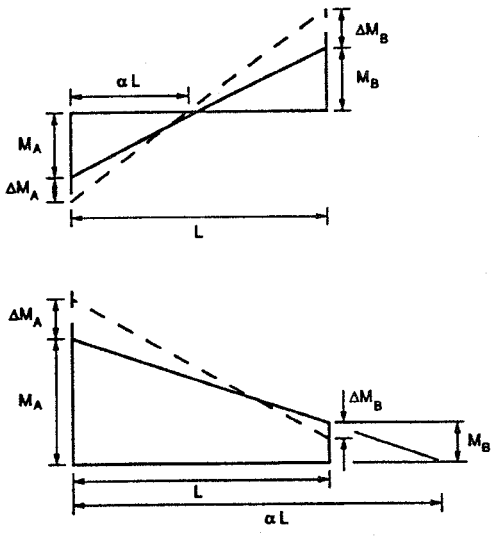

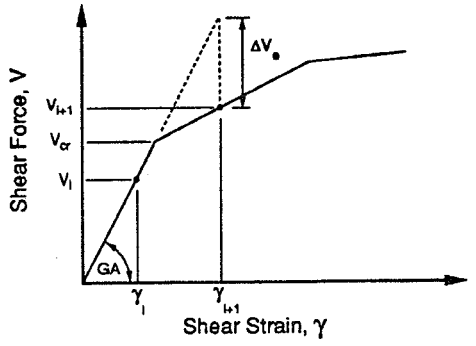

Figure 7 Treatment of unbalanced forces in shear spring of pedestal region

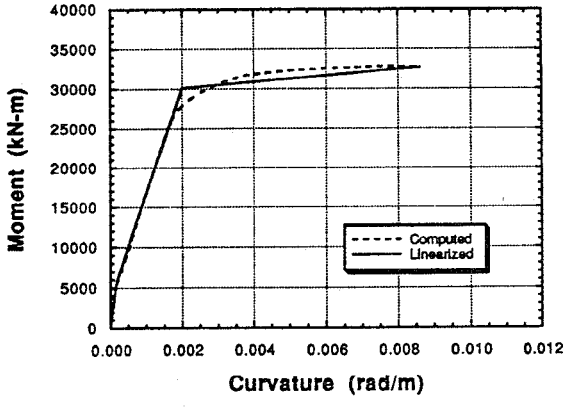

Figure 8 Moment–curvature relationship and trilinear representation for lower level columns

deformation relationship as input information for the analysis. To obtain this relationship, an inelastic finite element analysis of the pedestal region was conducted using the program FEM/I[7]. Modelling was accomplished with a four-node isoparametric quadrilateral element and a 2×2 Gaussian integration scheme. Concrete and reinforcing steel were modelled separately in an overlaid model in which strain compatibility was enforced at the nodes. The concrete is represented by an orthotropic material model and includes tension stiffening, compression softening, strain softening and a degrading modulus unloading rule. Distributed cracking occurs when the principle tensile strain at a Gauss point exceeds the specified cracking strain. Cracks form perpendicular to the direction of principal tensile strain. Compressive strength reduction after tensile cracking is accounted for as well as compressive strength increase due to lateral confinement. The reinforcing steel is represented by an orthotropic material model with a bilinear stress–strain relationship and includes unloading. Different material properties were used to describe the pedestal, negative beam reinforcement and beam-column joint region. The pedestal model was loaded with fixed gravity load and shear applied at the top of the pedestal in both directions. The finite element model of the pedestal region, the resulting shear force–deflection, and the equivalent trilinear model used in the final IDARC analysis are all shown in *Figure 9*.

The ultimate shear strain was determined by calibration with lateral load tests performed on an undamaged portion of the Cypress Viaduct reported by Housner[3]. A plane of failure extending from the edge of the shear key to the negative beam reinforcement was observed. Comparison of this analytical prediction of failure of the pedestal region compares favourably with observed failure[8].

3. Validation of model

The structural model of the Cypress Viaduct, consisting of the flexibility based beam-column elements and the shear panel representation of the pedestal region in conjunction with the force–deformation properties prescribed in the previous section and the assumed hysteretic model parameters, was validated through numerous analyses and by comparison with the observed behaviour. First, an elastic gravity load analysis was conducted to determine the appropriate number of beam sections to use to adequately represent beam flexure and to determine if inelastic action resulted from gravity load alone. Next, the fundamental frequency was computed to compare with results from ambient and forced vibration tests conducted on a three-bent portion of the Cypress Viaduct that remained standing. Finally, a lateral load analysis was conducted to compare with test results of the same three-bent portion of the structure loaded laterally to failure.

3.1. Gravity load analysis

An elastic analysis was conducted to obtain the moment and shear diagrams for the type B1 bent of the Cypress Viaduct under gravity load only. The analysis revealed that the cracking moment was exceeded in several locations. Thus, the gravity load had to be included in subsequent IDARC analyses as a dynamic load, so that all inelastic action would be included. The gravity load was applied as an incrementally increasing vertical acceleration in the following form

$$A_v = 0.5\left(1 - \cos\pi\frac{t}{t_o}\right) \tag{11}$$

where A_v is the vertical acceleration expressed in g, t is the

Table 1 Beam properties

		Flexural rigidity* (kN-m²)	Cracking moment (kN-m)	Yield moment (kN-m)	Yield curvature (rad/mm)
Lower level					
Left	(positive)	4.31E+07	5.16E+03	7.97E+03	9.02E–07
	(negative)	4.31E+07	5.32E+03	1.55E+04	9.89E–07
Right	(positive)	4.31E+07	5.54E+03	2.51E+04	1.13E–06
	(negative)	4.31E+07	2.09E+03	2.33E+04	8.27E–07
Upper level					
Left	(positive)	4.31E+07	5.06E+03	9.81E+03	9.42E–07
	(negative)	4.31E+07	4.98E+03	6.16E+03	9.10E–07
Right	(positive)	4.31E+07	5.79E+03	3.41E+04	1.31E–06
	(negative)	4.31E+07	2.44E+03	2.71E+03	8.43E–07

*Product of Young's modulus and moment of inertia (*EI*)

Table 2 Column properties

	Flexural rigidity (kN-m²)	Cracking moment (kN-m)	Yield moment (kN-m)	Yield curvature (rad/mm)
Lower level				
Top	2.40E+07	5.69E+03	3.01E+04	2.02E–06
Bottom	2.40E+07	5.69E+03	3.01E+04	2.02E–06
Upper level				
Top	6.66E+06	2.17E+03	1.02E+04	2.85E–06
Bottom	2.93E+06	1.38E+03	7.28E+03	4.09E–06

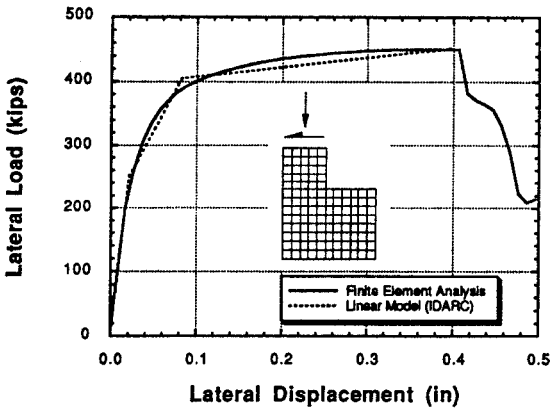

Figure 9 Trilinear representation of force–deformation relation for pedestal region; (inset: finite element model of pedestal region)

time increment, and t_o is the duration of the ramp. If t_o is selected to be at least twice the fundamental period, dynamic application of the gravity load will not excite the structure and there will be little free vibration. The fundamental period of the Cypress Viaduct bent under study was found to be approximately 0.4 s; therefore, the gravity load was applied over 2 s. Any resulting small vibrations were permitted to damp out for 2 s before the earthquake accelerations were applied in subsequent runs.

3.2. *Vibration analysis*

Ambient vibration tests were conducted on a three-bent portion of the Cypress Viaduct that remained standing after the Loma Prieta earthquake[3]. Measurements were made on the span between bents 45 and 46. The bents were of the type B1 configuration and were reported to be relatively undamaged. The measured first mode frequency was found to be 2.5 Hz. Forced vibration tests were also conducted on the three-bent test structure prior to static lateral load tests. Again the first-mode frequency was found to be 2.5 Hz.

To compare with the measured first-mode frequency, a time-history analysis was conducted on the IDARC model of type B1 bent. First, gravity load was applied dynamically as described in the previous section and the vibrations were allowed to damp out. Next, the Outer Harbor Wharf ground acceleration record, scaled by one half, was applied. This was done to approximate the minor damage that resulted from the earthquake. Finally, the time-history analysis was conducted for an additional 4 s (no applied accelerations) to allow the structure to vibrate freely. A record of the computed second-level accelerations during the last 4 s of free vibration and the results of a fast Fourier transform (FFT) on the last 4 s of the computed second-level accelerations are shown in *Figure 10*. The lowest modal frequency was found to be 2.48 Hz which compares favourably with the measured value of 2.5 Hz.

3.3. *Lateral load test*

The three-bent test structure mentioned above was tested to failure by loading all three bents laterally with hydraulic jacks[3]. To simulate this loading condition, the IDARC program was modified to permit application of the lateral load following application of the gravity and earthquake loads dynamically. The results of the IDARC analysis and the recorded response during testing are shown in *Figure 11*. Again, the agreement between the analysis and the test results is good.

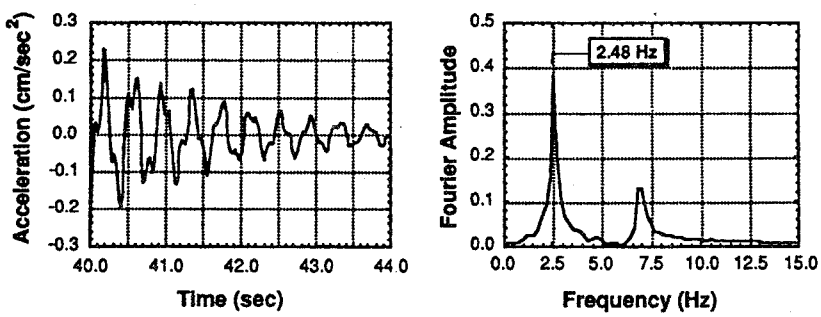

Figure 10 Validation of fundamental natural frequency: free vibration time history and Fourier amplitude

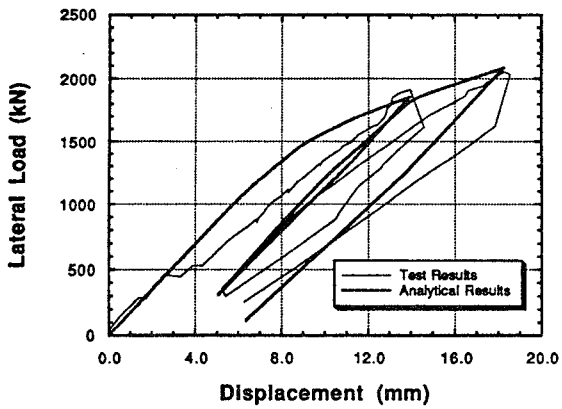

Figure 11 Static lateral load test: computed versus observed behaviour

The lateral load test was stopped when cracking in the pedestals was observed. Thus, the capacity of one bent, as determined by failure of the pedestal region, was reported to be 2070 kN (465 kips). Assuming both pedestals share the load equally, this corresponds to a single pedestal capacity of 1035 kN (233 kips). The capacity of the pedestal, loaded to produce shear in the same direction as that caused by gravity load, was determined by inelastic finite element analysis to be 2000 kN (450 kips). The inelastic gravity load analysis predicted a shear of 980 kN (220 kips) in the pedestal. The expected lateral failure load of one pedestal is, therefore, obtained by subtracting the gravity shear from the predicted shear capacity, or $2000 - 980 = 1020$ kN (230 kips). A comparison of this value with the measured capacity of 1035 kN (233 kips) indicates that the pedestal capacity, as determined by inelastic finite element analysis is reasonable.

4. Damage analysis of the Cypress Viaduct

The Loma Prieta earthquake which occurred on 17 October 1989, was a magnitude 7.1 earthquake and its epicentre was located near Santa Cruz, California. Ground acceleration records were available from three sites near the Cypress Viaduct; Emeryville to the north, Outer Harbor Wharf to the west, and a two-storey office building in Oakland, to the east. While all three records show strong similarity, the Outer Harbor Wharf Record was selected for the dynamic analyses in this study since it was considered to be the least influenced by nearby structures.

The Outer Harbor Wharf horizontal strong-motion records, with a peak horizontal acceleration of 0.33 g, were transformed to 94° which is transverse to the alignment of that portion of the Cypress Viaduct that collapsed. The IDARC model of the Cypress bent was subjected to both horizontal and vertical ground motions in addition to gravity loading as described earlier. A review of component damage indices following the analysis revealed that the first element to fail was the left-side pedestal (modelled as a shear wall panel element). *Figure 12* shows a three-part plot of the horizontal acceleration record, left-side pedestal shear force versus time, and pedestal damage index versus time. It can be seen that the analysis predicts a component damage index of 1.0, which corresponds to failure, at approximately 12.5 s after the earthquake had started. Analysis results beyond failure of an element are meaning-

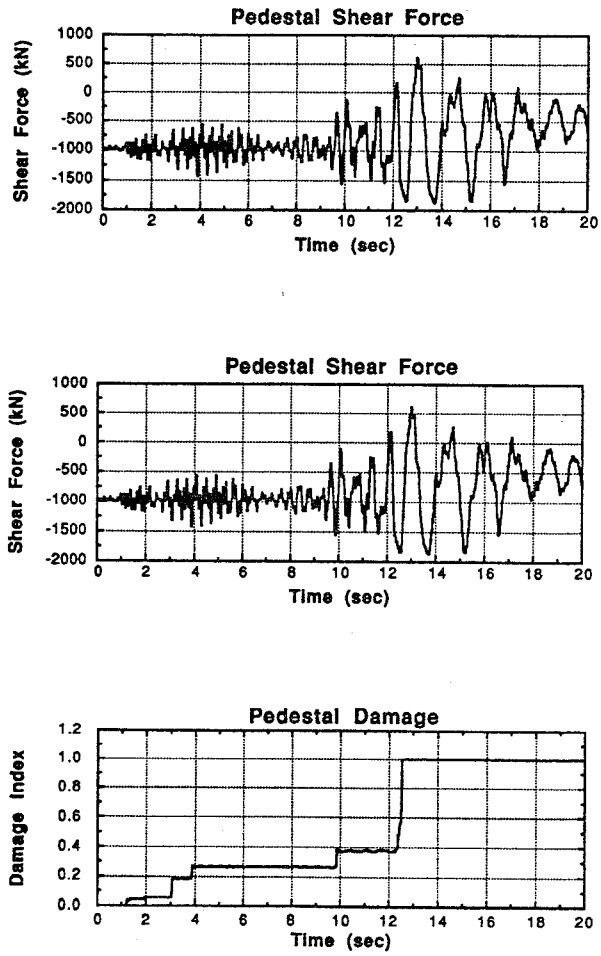

Figure 12 Analytical simulation of progressive damage for left pedestal

less since the program is not capable of accounting for the drastic changes in structural configuration that result from a brittle shear failure.

The upper level girder-to-column joint sustained flexural cracking and yielding of the reinforcement, but did not fail prior to failure of the pedestals. Component damage indices for the upper level girder at the left girder-to-column joint increased noticeably about the time the first large ground acceleration occurred (around 12.5 s) but were still well below a value that would suggest failure at the girder-to-column joint. The analysis, of course, was not able to simulate the subsequent failure that, according to Housner[3], was a result of the upper level columns being thrust outward as the upper level deck collapsed onto the lower level deck.

5. Conclusions

Many investigators have surveyed the collapsed Cypress Viaduct and have reported on their findings. The most comprehensive documentation is the report to Governor George Deukmejian titled 'Competing against time'[3] which draws on the observations and analyses of many investigators. The failure sequence described by Housner[3] is in agreement with the results of the present study. Failure of one pedestal was followed quickly by failure of the other pedestal. The upper level columns, having lost their vertical support, splayed outward as the upper level roadway collapsed onto the lower level. It is also noted that

> 'The upper girder-to-column joint sometimes failed completely, but in other cases was just severely cracked. Almost all the damage in this upper joint seems to have been produced as a result of the collapse of the upper deck onto the lower deck.'[3]

The significance of this observation is that the upper girder-to-column connections, while probably suffering flexural cracking as a result of inelastic frame action, did not fail prior to shear failure of the pedestals. Had the upper girder-to-column connections failed prior to pedestal failure, by either compressive crushing or bar pullout, the collapse would have likely been in a lateral rather than a vertical direction.

The maximum moment in the upper level girder-to-column joint is determined from the shear capacity of the pedestals, assuming that no moment is transmitted by the shear keys. The maximum moment is simply the product of the maximum shear capacity of one pedestal, 2000 kN (450 kips) times the upper level column height, 5.1 m (16.75 ft), assuming centreline dimensions, or approximately 10 220 kN-m (90 450 in-kips). This moment is seen to exceed the computed negative yield moment of approximately 6160 kN-m (54 500 in-kip), but is less than the ultimate moment. On the basis of these calculations, one would expect that the upper level girder-to-column joint would experience moments in excess of member cracking and yielding but the ultimate moment, determined by compressive crushing, would not be reached prior to shear failure of the pedestals.

It should be emphasized that the model of the Cypress Viaduct type B1 bent developed in this study was not changed or modified to produce better agreement with the experimental results. The agreement of the computed and measured first mode frequency indicated accurate modelling of the structural stiffness and mass distribution as well as approximated stiffness reduction due to cracking.

Based on the results of this study, it may be stated that the performance of existing concrete structures subjected to strong ground shaking can be predicted if reliable component models are used in conjunction with reliable estimates of member properties (including stiffness, strength and ductility). It is important, however, to recognize all potential failure modes and to ascertain that the analytical models handle them in a consistent manner.

Acknowledgments

The IDARC computer program was developed with funds provided by the National Center for Earthquake Engineering Research (NCEER) which in turn is supported by the National Science Foundation and the State of New York. Professor Andrei Reinhorn of the State University of New York at Buffalo along with the primary author of this paper supervised the IDARC developments. The modifications to the program to support this study and the specific results presented here were supported by the U.S. Geological Survey.

References

1 Kunnath, S. K., Reinhorn, A. M. and Abel, J. F. 'A computational tool for evaluation of seismic performance of reinforced concrete buildings', *Comput. Struct.* 1991, **41**, 157–173

2 Kunnath, S. K., Reinhorn, A. M. and Lobo, R. F. 'IDARC Version 3.0 – a program for inelastic damage analysis of reinforced concrete structures', *Technical Report NCEER 92-0022*, National Center for Earthquake Engineering Research, State University of New York, Buffalo, 1992

3 Housner, G. W. 'Competing against time. *Report to Governor George Deukmejian from the Governor's Board of Inquiry on the 1989 Loma Prieta Earthquake*, State of California', 1990

4 Gross, J. L. and Kunnath, S. K. 'Application of inelastic damage analysis to double-deck highway structures', *Report NISTIR 4857*, U.S. Department of Commerce, National Institute of Standards and Technology, Gaithersburg, Maryland, 1992

5 Park, Y. J., Reinhorn, A. M. and Kunnath, S. K. 'IDARC – inelastic damage analysis of reinforced concrete frame–shear-wall structures', *Technical Report NCEER-87-0008*, State University of New York at Buffalo, NY, 1987

6 Park, Y. J., Ang, A. H.-S. and Wen, Y. K. 'Seismic damage analysis and damage limiting design of R/C buildings', *Civil Engineering Studies Report SRS 516*, University of Illinois, Urbana, IL, 1984

7 Ewing, R. D., El-Mustapha, A. M. and Kariotis, J. C. 'FEM/I: a finite element computer program for the nonlinear static analysis of reinforced masonry buildings', *Report 2.2-1*, Ewing/Kariotis/Englekirk & Hart, Ewing and Associates, California, 1991

8 Nims, D. K., Miranda, E., Aiken, I.D., Whittaker, A.S. and Bertero, V.V. 'Collapse of the Cypress Street Viaduct as a result of the Loma Prieta Earthquake', *Report UBC/EERC-89/16*, University of California at Berkeley, CA, 1989